***Supporting Information***

# Building Pyridinium Molecular Wires as Axial Ligands for Tuning the Electrocatalytic Activity of Iron Phthalocyanines for the Oxygen Reduction Reaction.

*Ana Pizarro†, Gabriel Abarca⊥, Cristian Gutiérrez-Cerón†, Diego Cortés-Arriagadaξ, Fabiano Bernardi‡, Cristhian Berrios†, Juan F. Silva†, Marcos C. Rezende†, José H. Zagal*†, Rubén Oñate†*, Ingrid Ponce†*.*

AUTHOR ADDRESSES † Facultad de Química y Biología, Universidad de Santiago de Chile. Avenida Libertador Bernardo O'Higgins 3363, Casilla 40, Correo 33, Santiago 9170022, Chile. ⊥Centro de Nanotecnología Aplicada, Facultad de Ciencias, Universidad Mayor, Chile. Camino la Pirámide 5750, Huechuraba 8580745, Santiago, Chile. ξ Programa Institucional de Fomento a la Investigación, Desarrollo e Innovación. Universidad Tecnológica Metropolitana. Ignacio Valdivieso 2409, P.O. Box 8940577, San Joaquín, Santiago, Chile. ‡ Institute of Physics, Universidade Federal do Rio Grande do Sul, Av. Bento Gonçalves, 9500, Porto Alegre, 91501-970, RS, Brazil.

AUTHOR INFORMATION

Corresponding Author

* ruben.paine@usach.cl * jose.zagal@usach.cl * ingrid.ponce@usach.cl

**Table of Contents.**

**Characterizations pyridinium *Up*.**

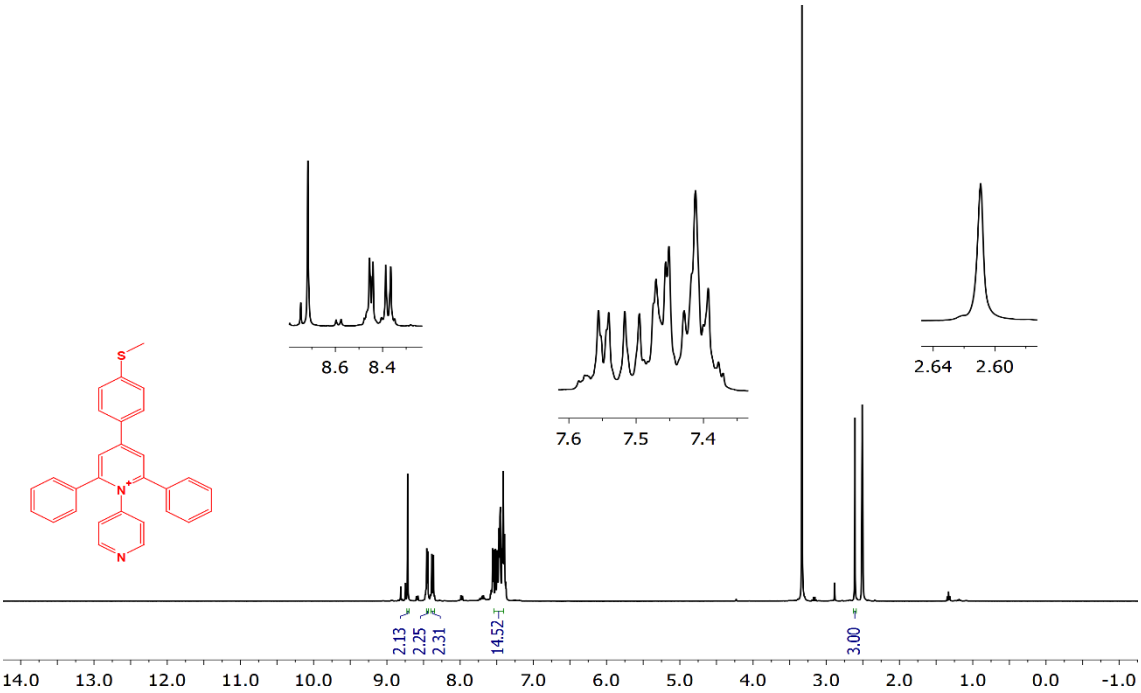


Figure S1. $^{1}$H NMR of *Up* pyridinium in DMSO-*d*6.

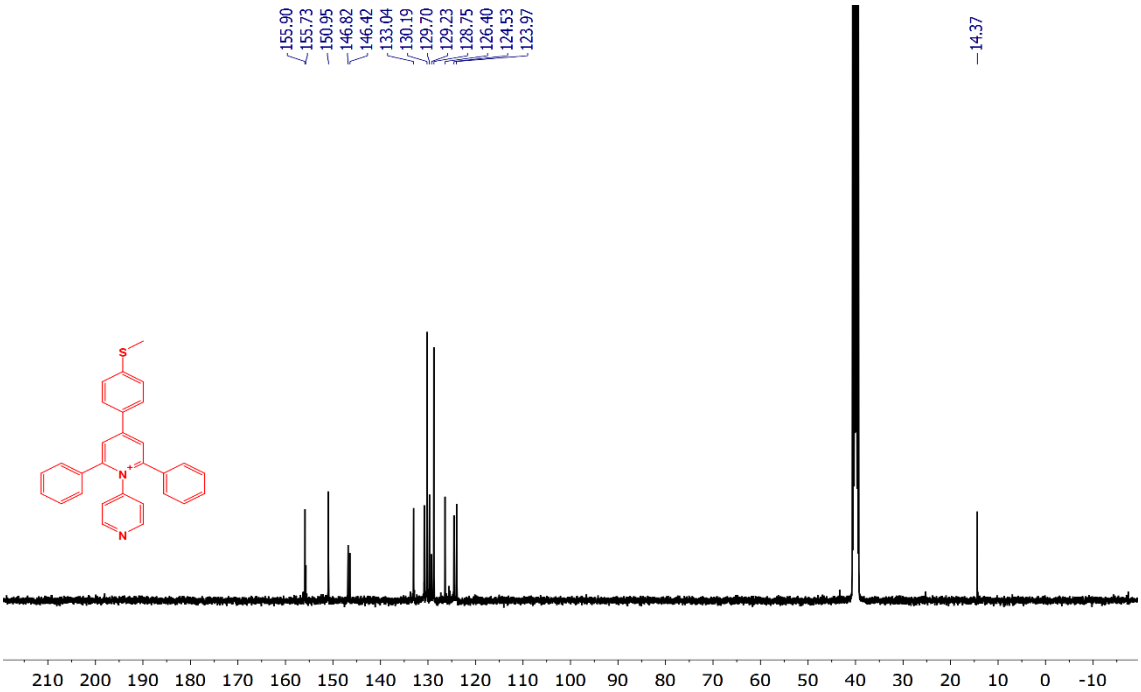


Figure S2. $^{13}$C NMR of *Up* pyridinium in DMSO-*d*6.

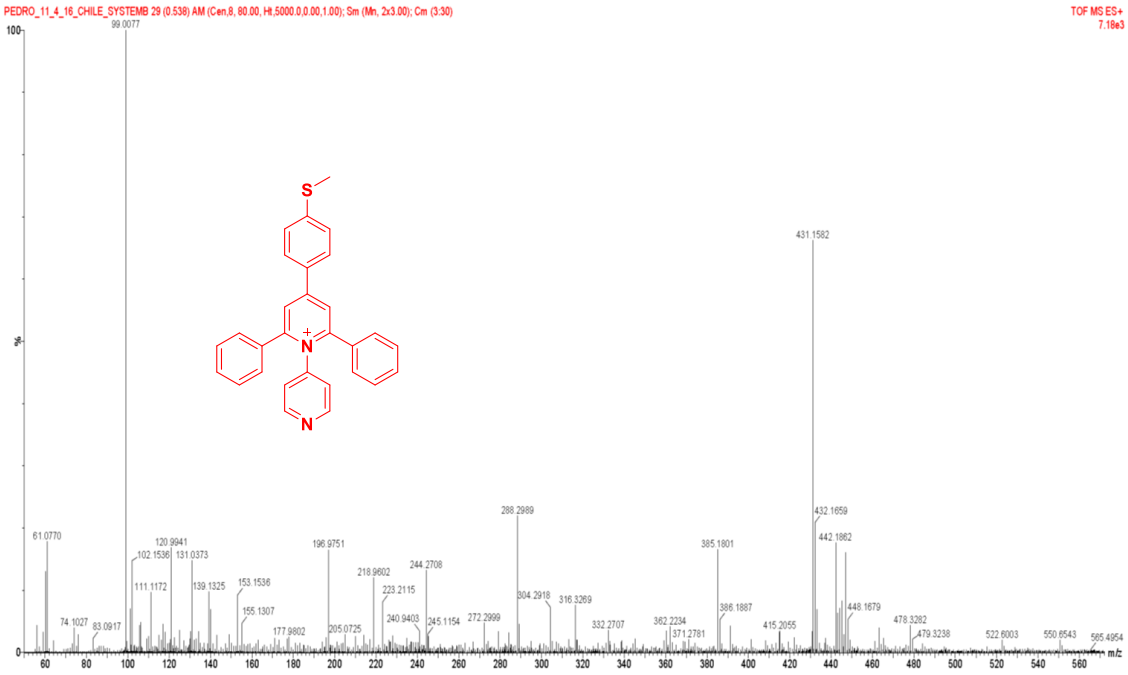


Figure S3. HRMS of *Up* pyridinium.

**Details of characterization of Self-assembled systems**

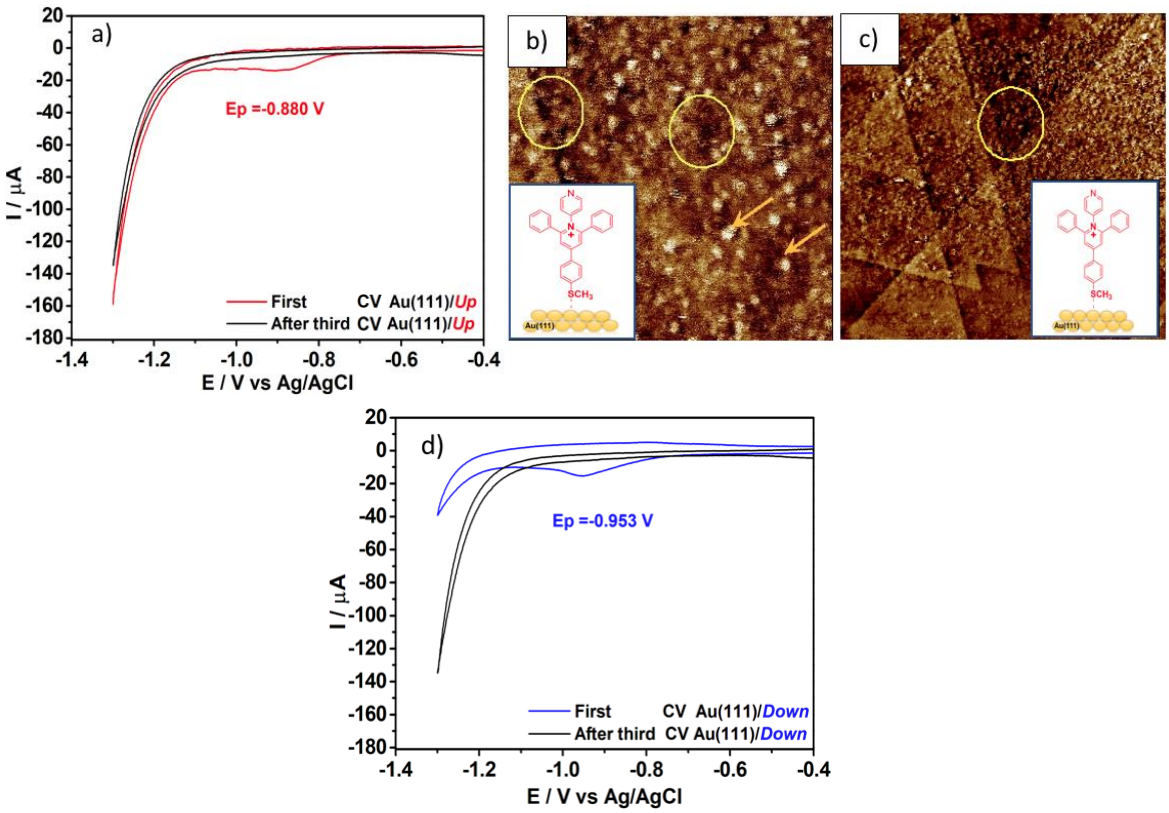


Figure S4. a) Electro-reductive desorption of pyridinium SAMs of *Au(111)/Up,* b) and c) height STM images of *Up* pyridinium molecular assemblies on the surface of Au(111), 30 x 30 nm. and 110 x 110 nm respectively. In both images there are pinholes (yellow circles) and clusters (yellow arrows), $I_t$=150 pA and $V_{Bias}$=0.92 V. d) Electro-reductive desorption of pyridinium SAMs of *Au(111)/Down*.

To obtain the corresponding experimental values to the Charge Density from reduction peak integration, $\boldsymbol{Q}$ (µC) and Surface Coverage, $\boldsymbol{\Gamma}$ (mol/cm$^2$) of each monolayer, the area under the curve of the electro-desorption process of each SAMs was integrated (cathodic peak in Figures S4) and was divided by the corresponding scan rate.[1] According to equation S.1,[2–4] was possible to obtain the corresponding Surface Coverage values for each SAMs.

$$\Gamma = \frac{Q}{n \times F \times A_r} \quad \text{(S.1)}$$

Where $n$ represents number of electrons transferred (≈1), $F$ the Faraday constant (96,485 $Cmol^{-1}$) and $A$ is the geometric surface area of the electrode ($cm^2$).

Table S1. Current peak, Charge density and surface coverage obtained from Electro-reductive desorption of pyridinium SAMs from the Au(111) surface.

| ***System*** | ***Current Peak*** **V vs Ag/AgCl** | ***Current Peak*** **V vs RHE** | ***Charge density*** **(μC)** | ***Surface Coverage*** **(x $10^{-10}$ mol/$cm^2$)** |
|---|---|---|---|---|
| *Au(111)/Up* | -0.880 | 0.081 | 28.40 | 4.62 |
| *Au(111)/Down* | -0.947 | 0.014 | 32.24 | 4.97 |

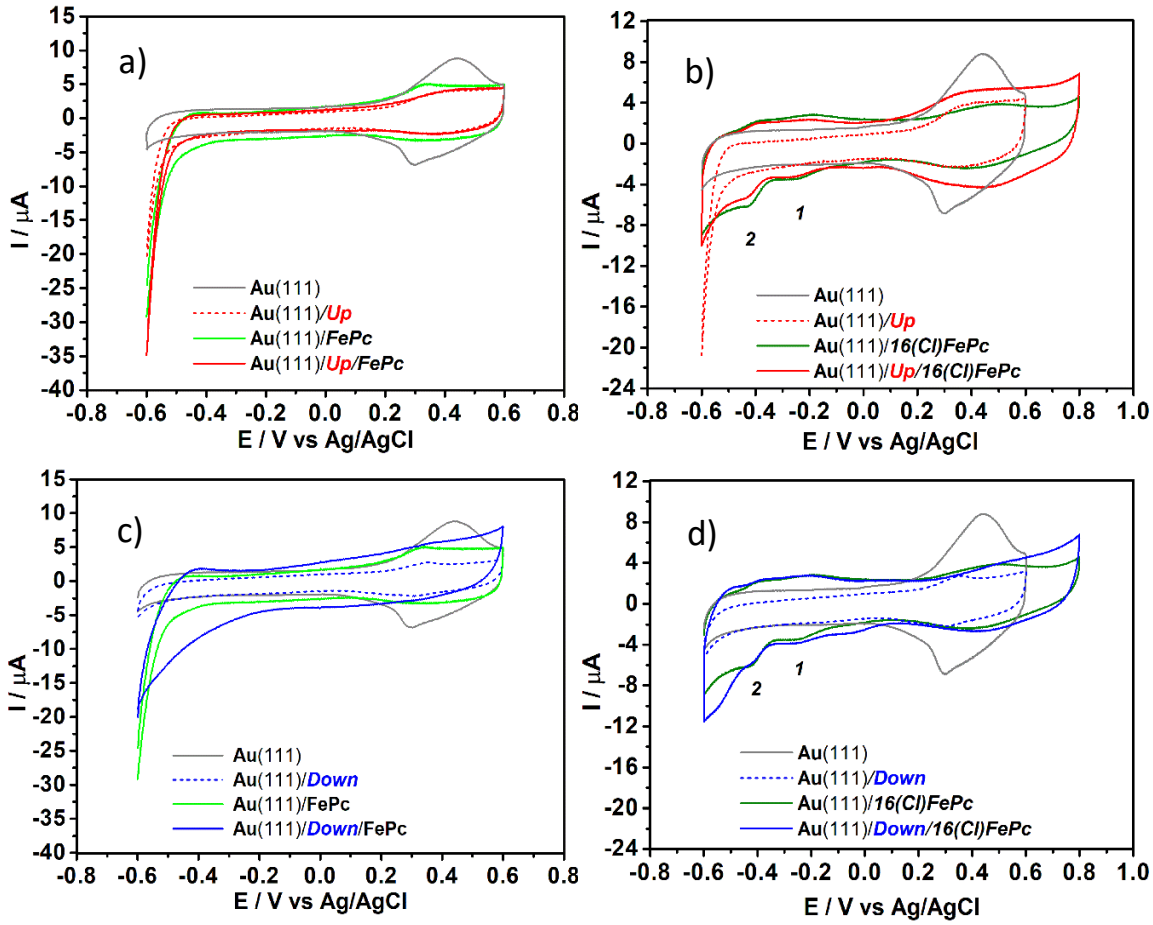


Figure S5. Cyclic voltammetric responses for Au(111), *Au(111)/Down(Up), Au(111)/FePcs and Au(111)/Down(Up)/FePcs systems*: a) *Au(111)/Up/FePc.* b) *Au(111)/Up/16(Cl)FePc*. c) *Au(111)/Down/FePc*. d) *Au(111)/Down/16(Cl)FePc.* Measurements conducted in *pH = 5* phosphate buffer solution satured whit $N_2$; 25 mV and 15 Hz, 25°C.

Table S2. Redox Potentials (**E°´**) for FePc and 16(Cl)FePc systems from Square wave voltammetric responses, Figure 2 in the main text.

| **Systems** | **E°´ Fe (II)/(I)[3] V vs Ag/AgCl** | | **E°´ Fe (III)/(II)[3] V vs Ag/AgCl** | | **E°´ Fe (II)/(I)[4] V vs RHE** | | **E°´ Fe (III)/(II)[4] V vs V vs RHE** | |
|---|---|---|---|---|---|---|---|---|
| | **pH = 5** | **pH =13** | **pH = 5** | **pH = 13** | **pH = 5** | **pH = 13** | **pH = 5** | **pH = 13** |
| *GPO/FePc[1]* vs SCE | -0.500 | -0.680 | +0.400 | -0.080 | | | | |
| *GPO/FePc[2]* | -0.463 | -0.643 | +0.437 | -0.043 | +0.027 | +0.317 | +0.927 | +0.917 |
| *Au(111)/FePc* | -0.460 | -0.637 | + 0.342 | -0.130 | +0.029 | +0.323 | +0.831 | +0.83 |
| *Au(111)/Down/FePc* | -0.450 | -0.627 | +0.373 | -0.099 | +0.039 | +0.333 | +0.862 | +0.861 |
| *Au(111)/Up/FePc* | -0.424 | -0.601 | +0.358 | -0.114 | +0.065 | +0.359 | +0.847 | +0.846 |
| *Au(111)/(16)ClFePc* | -0.412 | -0.589 | +0.224 | ----- | +0.078 | +0.371 | +0.714 | ----- |
| *Au(111)/Down/(16)ClFePc* | -0.408 | -0.585 | +0.224 | ----- | +0.082 | +0.375 | +0.714 | ----- |
| *Au(111)/Up/(16)ClFePc* | -0.404 | -0.581 | +0.224 | ----- | +0.086 | +0.379 | +0.714 | ----- |

*1 Data taken from Pourbaix Diagram. Reference* [5]

*2 Corrected data to Ag/AgCl reference electrode. Equation (S.2)*

*3 Extrapolated data to pH=13, Equation (S.3) and (S.4), for FePc systems on Gold surface.*

*4 Corrected data to RHE reference electrode.*

$$\boldsymbol{E_{Redox}\, Fe^{II/I\ or\ III/II}pH(x) = \left(E_{Redox}\, Fe^{II/I\ or\ III/II}pH(x) - (-0.0366V)\right)} \qquad \textbf{(}S.2\textbf{)}$$

Where -0.0366 V is the difference between Ag/AgCl (KCl; 3M) and SCE reference electrodes.

$$\boldsymbol{E_{Redox}\, Fe^{II/I}pH(13) = \left(E_{Redox}\, Fe^{II/I}pH(5) - (3x0.059V)\right)} \qquad (S.3)$$

The FePc/GPO Pourbaix diagram shows the possible Fe species presents under different conditions of pH and potential. The reversible Fe(II)/(I) redox couple is essentially pH independent in the range from pH=8 to pH=13. From pH=8 to pH=1, the Fe(II)/(I) redox couple shifts 0.059 V per *pH* unit.

$$\boldsymbol{E_{Redox}\, Fe^{III/II}pH(13) = \left(E_{Redox}\, Fe^{III/II}pH(5) - (8x0.0059\, V)\right)} \qquad (S.4)$$

The Fe(III)/(II) reversible redox couple shows pH dependence in a wide range of pH values, essentially from pH=13 to pH=1, It shows a Nernstian shift potential of 0.059 V per pH unit.

**XPS measurements.**

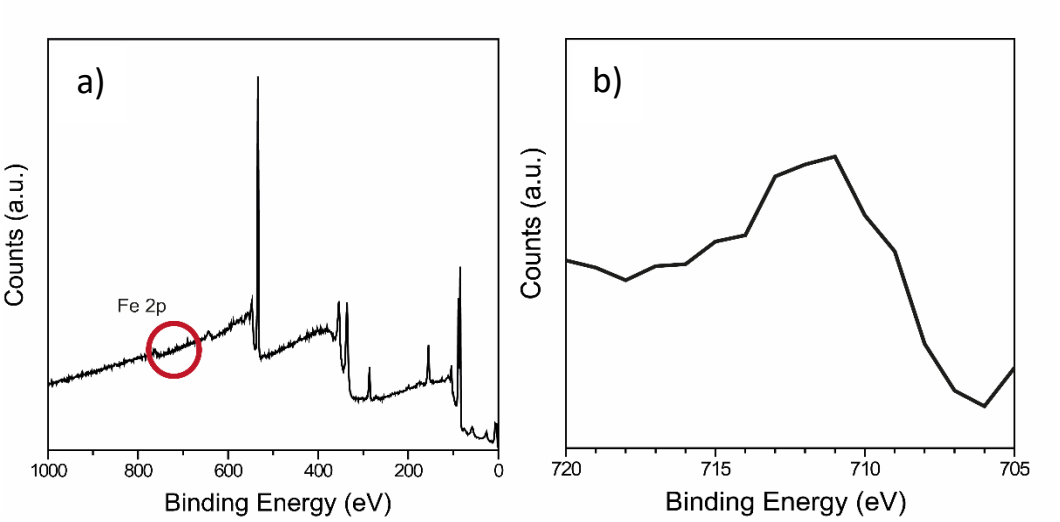


Figure S6. a) Long scan XPS spectra of Au/up/FePc. b) Fe $2p_{3/2}$ XPS spectra of the *Au(111)/Up/FePc* system with hν = 1840 eV.

In order to obtain information about the chemical surface of *Au(111)/Up/FePc* composite, XPS measurements were performed at Fe $2p_{3/2}$ region, using SXS beamline (LNLS). The broad Fe $2p_{3/2}$ signal indicates the presence of Fe in different valence states.

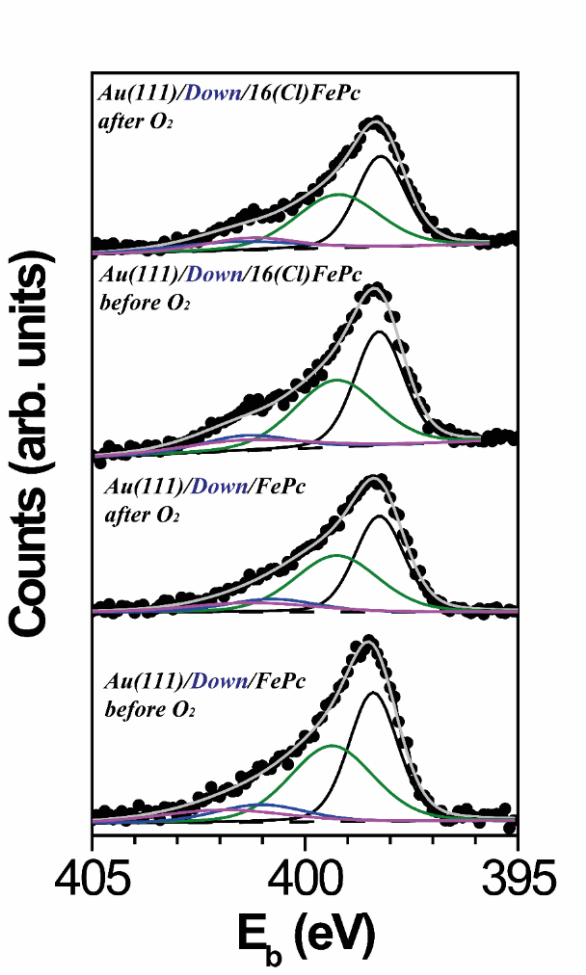


Figure S7. XPS measurements at the N 1s region of *Au(111)/Down/FePc* and *Au(111)/Down/16(Cl)FePc* before and after $O_2$ treatment at RT. The black points represent the experimental data and the gray line represents the best fitting found. At the N 1s region the black, green, blue and magenta solid lines represent the C-N=C, N-Fe (Pc), N pyridine and N pyridinium chemical components, respectively.

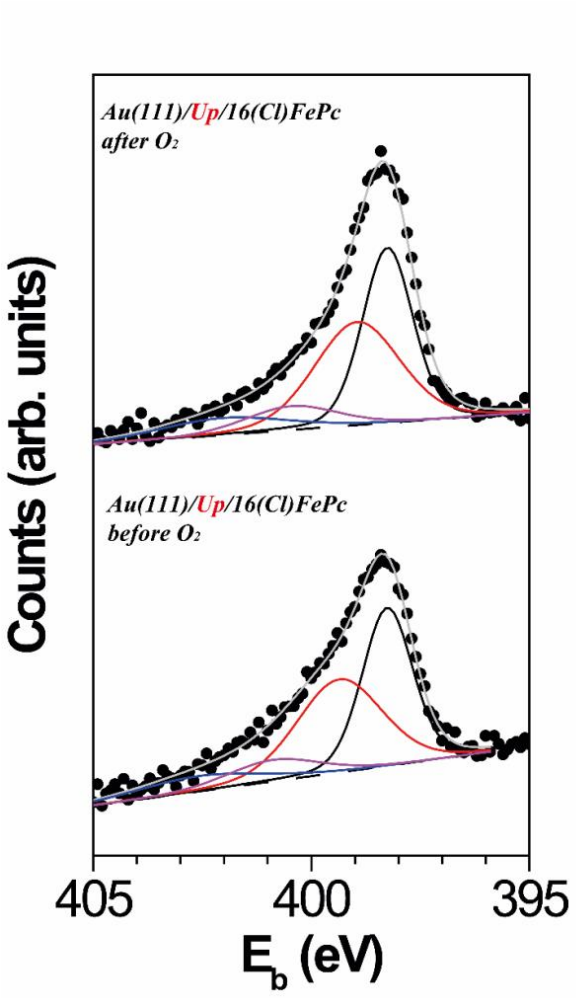


Figure S8. XPS measurements at the N 1s region of *Au(111)/Up/16(Cl)FePc* before and after $O_2$ treatment at RT. The black points represent the experimental data and the gray line represents the best fitting found. At the N 1s region the black, green, blue and magenta solid lines represent the C-N=C, N-Fe (Pc), N pyridine and N pyridinium chemical components, respectively.

Table S3– Binding energies values of the different chemical components found in the XPS measurements for the N 1s electronic level before and after treatment with $O_2$.

| | C-N=C before $O_2$ eV | C-N=C after $O_2$ eV | N-Fe(Pc) before $O_2$ eV | N-Fe(Pc) after $O_2$ eV | N-pyridine before $O_2$ eV | N-pyridine after $O_2$ eV | N-pyridinium before $O_2$ eV | N-pyridinium after $O_2$ eV |
|---|---|---|---|---|---|---|---|---|
| ***Au(111)/Down/FePc*** | 398.4 | 398.3 | 399.4 | 399.3 | 401.0 | 400.8 | 401.9 | 401.3 |
| ***Au(111)/Down/16(Cl)FePc*** | 398.3 | 398.2 | 399.3 | 399.2 | 401.4 | 401.3 | 401.4 | 401.6 |
| ***Au(111)/Up/16(Cl)FePc*** | 398.3 | 398.3 | 399.4 | 399.0 | 400.9 | 400.5 | 402.6 | 402.0 |

**Details of reduction of molecular oxygen.**

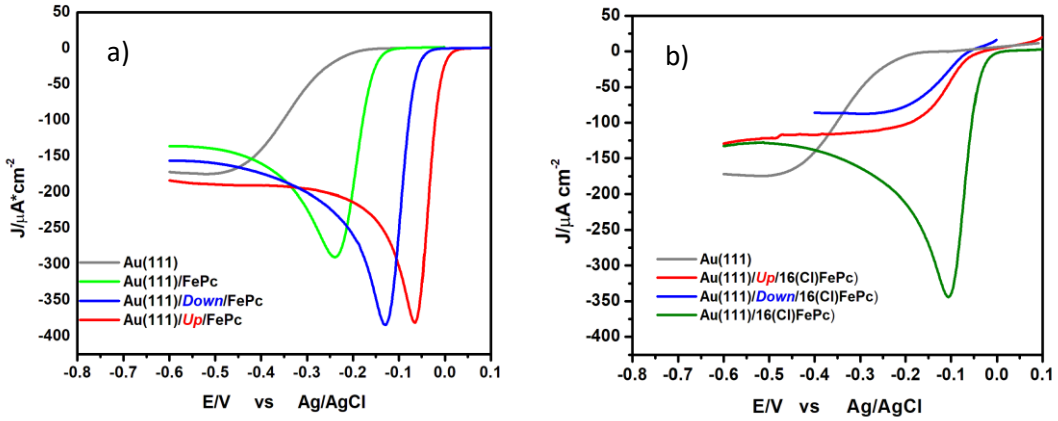


Figure S9. Linear sweep voltammetry for $O_2$ reduction, scan rate=0.005 V/s, NaOH 0.1 M $O_2$ saturated solution, T=25°C. a) FePc systems. b) 16(Cl)FePc systems.

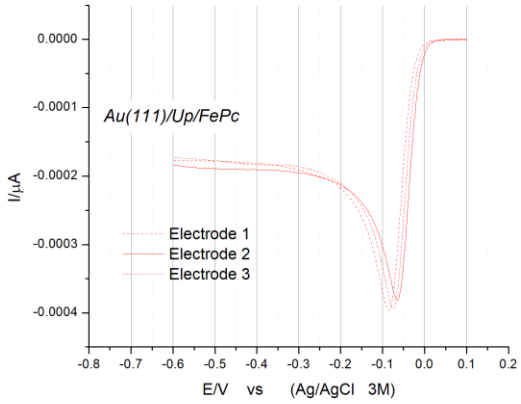


Figure S10. Linear sweep voltammetry for $O_2$ reduction, scan rate=0.005 V/s, NaOH 0.1 M $O_2$ saturated solution, T=25°C. *Au(111)/Up/FePc* system (three different electrodes).

The number of electrons for $O_2$ reduction process in each system have been determined by Randles-Sevcik equation[6] for irreversible processes and diffusion controlled, where "*n*" are the electrons transferred per molecule.

Parameter $n^{3/2} = Ip/137.887$

The peak currents, *Ip* was taken from cyclic voltammetry at 50 mV/s in NaOH 0.1 M; T=25°C.

Table S4. Peak current value (*Ip*) of cyclic voltammetry and number of electrons value (*n*) obtained for ORR on all systems studied in 0.1 M NaOH at 25°C.

| **System** | ***Ip* (μA /cm$^{2)}$** | ***n*** | ***n*$^{3/2}$** |
|---|---|---|---|
| *Au(111)* | 390 | 2.00 | 2.8284 |
| *Au(111)/FePc* | 560 | 2.54 | **4.0610** |
| *Au(111)/Down/FePc* | 1070 | 3.91 | 7.7599 |
| *Au(111)/Up/FePc* | 1210 | 4.25 | 8.7750 |
| *Au(111)/16(Cl)FePc* | 1100 | 3.99 | 7.9775 |
| *Au(111)/Down/16(Cl)FePc* | 460 | 2.23 | 3.3300 |
| *Au(111)/Up/16(Cl)FePc* | 500 | 2.70 | --- |

This table was constructed assuming that Au(111) is a pure 2-e ORR catalyst so *n=2* is assigned to this surface so n for the other surfaces was estimated from the maximum currents (*Ip*). A pure 4 electron catalyst should exhibit a maximum current exactly twice that for Au(111).

Example of calculation: for *Au(111)/FePc Ip* is 560 μA so $n^{3/2}$ = 560/137.887 = **4.0610**

**Computational Methods and Details of theoretical calculations.**

Table S5. Interaction energies for the ligand-complex and (ligand-complex)–$O_2$ interactions, in addition to selected bond lengths. Calculations were performed at the PBE-D3/Def2-SVP level of theory.

| System | $d_{O2\text{-}Fe}$ (Å) | $d_{N\text{-}Fe}$ (Å) | $E_{int}$ (eV) |
|---|---|---|---|
| *Down*/FePc | -- | 1.86 | -1.09 |
| *Down*/16(Cl)FePc | | 2.17 | -0.99 |
| *Down* /FePc-$O_2$ | 1.95 | 2.00 | -0.19 |
| *Down* /16(Cl)FePc-$O_2$ | 1.79 | 2.18 | -0.15 |
| *Up*/FePc | -- | 1.87 | -1.11 |
| *Up*/16(Cl)FePc | -- | 2.21 | -1.22 |
| *Up*/FePc-$O_2$ | 1.93 | 2.02 | -0.28 |
| *Up*/16(Cl)FePc-$O_2$ | 1.93 | 2.03 | -0.37 |
| FePc-$O_2$ | 1.73 | -- | -0.43 |
| 16(Cl)FePc-$O_2$ | 1.74 | -- | -0.45 |

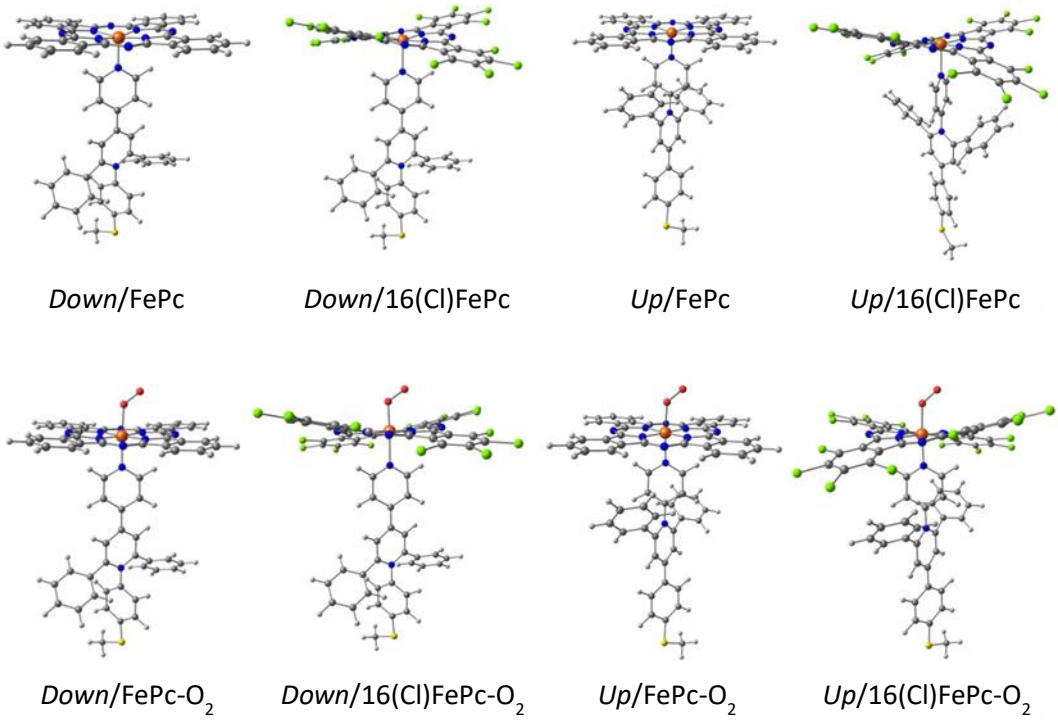


Figure S11. Optimized molecular structures of the ligand-complex and *(ligand-complex)–$O_2$* systems. Calculations were performed at the PBE-D3/Def2-SVP level of theory.

## References

(1) Yoshimoto, S.; Ono, Y.; Kuwahara, Y.; Nishiyama, K.; Taniguchi, I. Structural Changes of 4,4′-(Dithiodibutylene)Dipyridine SAM on a Au(111) Electrode with Applied Potential and Solution PH and Influence of Alkyl Chain Length of Pyridine-Terminated Thiolate SAMs on Cytochrome c Electrochemistry. *J. Phys. Chem. C* 2016, 120, 15803–15813.

(2) Pilloud, D. L.; Chen, X.; Dutton, P. L.; Moser, C. C. Electrochemistry of Self-Assembled Monolayers of Iron Protoporphyrin IX Attached to Modified Gold Electrodes through Thioether Linkage. *J. Phys. Chem. B* 2000, 104, 2868–2877.

(3) Vericat, C.; Vela, M. E.; Benitez, G.; Carro, P.; Salvarezza, R. C. Self-Assembled Monolayers of Thiols and Dithiols on Gold: New Challenges for a Well-Known System. *Chem. Soc. Rev.* 2010, 39, 1805.

(4) Ozoemena, K. I.; Nyokong, T. Comparative Electrochemistry and Electrocatalytic Activities of Cobalt, Iron and Manganese Phthalocyanine Complexes Axially Co-Ordinated to Mercaptopyridine Self-Assembled Monolayer at Gold Electrodes. *Electrochim. Acta* 2006, 51, 2669–2677.

(5) Zagal, J.; Páez, M.; Tanaka, A. A. A.; dos Santos, J. R. R.; Linkous, C. A. A. Electrocatalytic Activity of Metal Phthalocyanines for Oxygen Reduction. *J. Electroanal. Chem.* 1992, 339, 13–30.

(6) Zagal, J. H.; Koper, M. T. M. Reactivity Descriptors for the Activity of Molecular MN4 Catalysts for the Oxygen Reduction Reaction. *Angew. Chemie Int. Ed.* 2016, 55, 14510–14521.